DISTRIBUTION OF IMPACT-GENERATED BOULDERS ON PLANETARY SURFACES: INFLUENCE OF TARGET FRACTURATION AND LITHOLOGY

N.C. Prieur[1,2] (nilscp@stanford.edu), B. Amaro[1], E. Gonzalez[3], L. Rubanenko[1,4], Z. Xiao[5], H. Kerner[6], S.C. Werner[2] and M.G.A. Lapôtre[1]. [1]Dpt. Earth & Planetary Sciences, Stanford U., USA. [2]Dpt. of Geosciences, U. Oslo, Norway. [3] Dpt. Geological Sciences, California State Polytechnic University Pomona, USA. [4]Dept. Civil & Environmental Eng., Technion, Israel. [5]Sun Yat-Sen University, China. [6] Sch. Computing & Augmented Intelligence, ASU, USA.

Introduction: On rocky surfaces, many boulders form as rock fragments ejected upon meteor impact and are deposited around impact craters. Some of those fragments are ejected with sufficient kinetic energy to create secondary craters, therefore increasing the density of impact craters and, in doing so, biasing surface ages estimated from crater counting. Thus, understanding boulder generation and ejection during crater formation offers a unique opportunity to correct such biases in surface age determinations [1]. However, few boulder fields have been investigated around impact craters [2–11]. Whereas valuable information was extracted from those studies, collected data are insufficient to systematically analyze the roles played by, e.g., impactor and target properties.

A major challenge to conducting such a systematic analysis is the enormous number of resolvable boulders often associated with a single impact structure. For example, fresh impact craters larger than a kilometer on the Moon were shown to host 10–100x10^3 boulders on their ejecta [6,11]. However, manual mapping of boulder populations has been the most commonly employed approach [5–11], despite its time-consuming nature. Automating boulder detection will be key to obtaining statistically significant and high-quality boulder statistics over large and varied planetary surfaces. To that end, we aim to train a convolutional neural network (CNN, referred to as BoulderNet) to detect boulders automatically on planetary surfaces [12].

Methods: First, we manually mapped boulders (here defined as rock fragments with distinct outlines and areas larger than 6x6 pixels, regardless of their degree of burial) on the surface of the Earth, Moon, and Mars from high-resolution imagery (drone, NAC [13], and HiRISE [14] images, respectively). Mapping was conducted on images of impact structures with different levels of crater degradation, terrain types, and solar incidence angles of 0–40° to minimize shadows. Boulder outlines were then converted to annotation labels and imported as input to the CNN along with their corresponding high-resolution 500x500 pixels images (for a total of 393 training image tiles). Next, we trained the instance segmentation Mask R-CNN model architecture [15]. The current best iteration of BoulderNet uses ResNet50 as a backbone and includes a number of augmentations, such as brightness, contrast, random 90° rotations, resolution resampling, and sharpening.

To quantify model performance, 130 test image tiles were randomly set aside. The Intersection over Union (IoU) of predicted boulders was then used as a performance metric. Here, we report IoUs of 50 and 75%, meaning that only predictions with IoUs larger than 0.50 and 0.75 are considered correct detections. Table 1 reports IoUs for terrestrial glacial erratics in the Sierra Nevada (37.1°N 119.0°W, drone image, CA, USA) and boulders inside and outside the Censorinus impact crater on the Moon (0.4°S, 32.7°E, NAC image M139694087LE). Inferred slopes in cumulative size-frequency space are consistent between manual and predicted boulders for medium and large boulder populations, even if not all boulders are detected.

BoulderNet was then used to investigate whether impact craters of similar diameters (and thus approximately same kinetic energy) generate identical boulder fragmentation patterns on the Moon. Specifically, we opted to focus on young and fresh (i.e., no visible degradation) ~2-km impact craters (well above the strength-gravity diameter transition [16]; ~100–300 m) in both lunar mare and highlands.

Rocky materials tend to generate fragments of sizes that roughly follow power-law distributions, $N(>D)=C.D^{-\beta}$, where N is the cumulative number of fragments with diameter > D, and β and C are constants. The slope parameter, β, varies with the fragmentation process and history [3]. To compare boulder populations, we fit such power laws to detected medium-large boulders (16^2 < A < 32^2, boulder diameters roughly between 7–24 m depending on image resolution).

Results: At the time of writing this abstract, we had conducted our analysis for 6 fresh lunar mare craters (Fig. 1), extending the mapping 1–2 radii away from the crater center. Results for additional mare and fresh highland craters will be presented at the conference. The boulder cumulative size-frequency distributions (BCSFD) are shown for each of those craters in Fig. 2. Based on our preliminary data, two preliminary conclusions can be drawn. First, the absolute number of boulders of a given size varies across craters, despite similar crater sizes and target lithology. Second, BCSFD slopes range from -3.24 to -4.73. The lowest and highest β values inferred here appear to result from over- and under-estimates due to poorer predictions in slightly more degraded craters. Excluding those two boulder populations, we find a slope of -3.64 to -4.13.

Discussion: Slope values of detected BCSFDs are consistent with published values for the slope of CSFDs of secondary craters (-4) around Langrenus [2] as well as with boulder populations in two highland craters (-3.8 to -5.3) from [9]. Furthermore, our preliminary results suggest that the absolute number of boulders varies despite the overall similar kinetic energy of the impactor and similar target lithology. Thus, initial conditions such as fracturation state prior to impact or impactor conditions could play a role in setting the maximum possible boulder size. The relative role of target lithology (maria vs. highlands) and fracturation state will be discussed in more detail at the conference.

Table 1. Intersection over Unions (IoUs) for boulder predictions for terrestrial glacial erratics in the Sierra Nevada (Earth) and boulders inside and outside the Censorinus impact crater (Moon). Boulders are divided into four size groups (all: > 6^2, small: 6^2 < A < 16^2, medium: 16^2 < A < 32^2, large: A > 32^2 sq. pixels).

Location	IoU	All (Precision/ Recall)	Small	Medium	Large
Earth	50 %	89/73	93/54	96/86	96/88
	75 %	77/63	65/38	94/84	94/87
Moon	50 %	75/41	78/38	88/52	100/72
	75 %	38/20	38/18	65/38	63/45

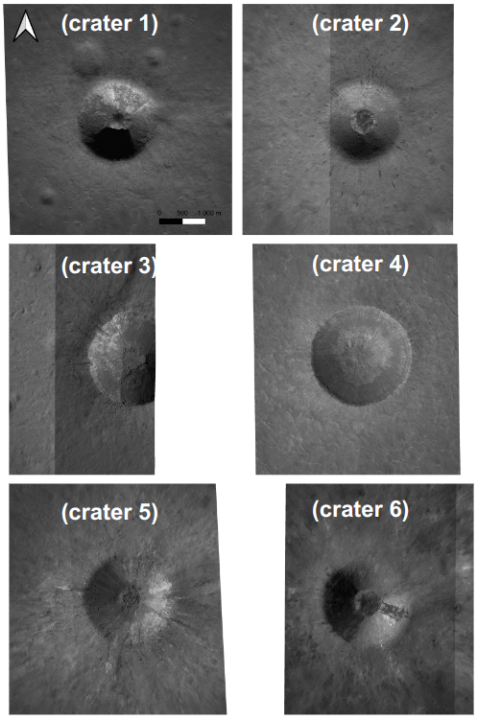

Fig 1. NAC images [13] of 6 fresh lunar mare craters with a diameter of 2.0±0.2 km.

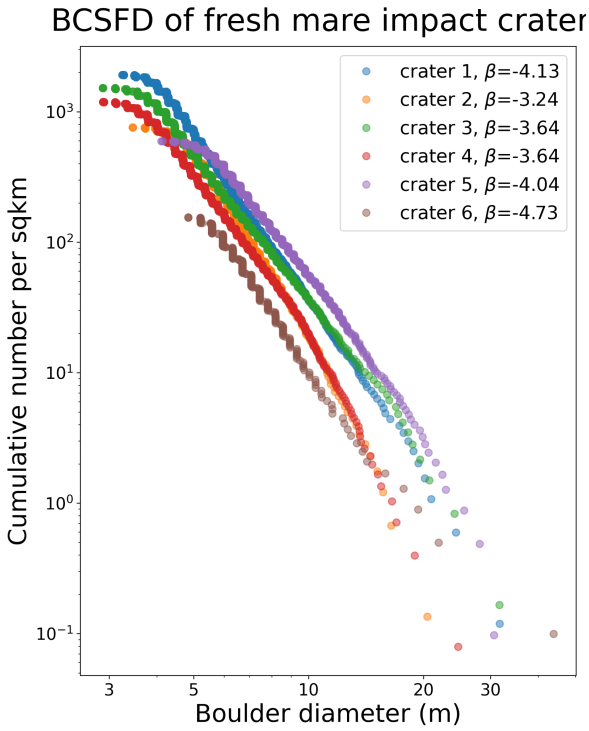

Fig 2. Cumulative boulder diameter size-frequency distribution of 6 fresh lunar mare craters with a diameter of 2.0±0.2 km. Only boulders within 1–2 radii from the crater center are selected. The slope parameters β are computed for medium-size boulders (16^2 < A < 32^2 sq. pixels) and depicted in the legend.

Acknowledgments: NCP acknowledges support from the European Commission (101030364) and Research Council of Norway (328597) through the MSCA-2020 Individual Global Fellowship hosted at Stanford University and the University of Oslo.

References: [1] Melosh (1984) Icarus 59. [2] Shoemaker (1965) JPL Tech. Rept. [3] Hartmann (1969) Icarus 10. [4] Vickery (1986) Icarus 67. [5] Bart & Melosh (2010) Icarus 209. [6] Krishna et al. (2016) Icarus 264. [7] Pajola et al. (2017) Icarus 296. [8] Pajola et al. (2019) PSS 165. [9] Watkins et al. (2019) JGR Planets 124. [10] Pajola et al. (2021) Universe 7, 82. [11] Mistick et al. (2022) Icarus 376. [12] Prieur et al. LPSC2022 #1835. [13] Robinson et al. (2010) Space Sc. Rev. 150. [14] McEwen et al. (2007) JGR Planets 112. [15] He et al. arXiv:1703.06870. [16] Holsapple (1993) Annu. Rev. Earth Planet Sci. 21.